JOURNAL OF SOLID STATE CHEMISTRY **124,** 309–318 (1996)
ARTICLE NO. 0242

Synthesis and *ab initio* Structure Determination from Powder X-Ray Diffraction Data of a New Metallic Mixed-Valence Platinum–Lead Oxide $PbPt_2O_4$

N. Tancret, S. Obbade, N. Bettahar,[1] and F. Abraham[2]

Laboratoire de Cristallochimie et Physicochimie du Solide, ENSCL-USTLille, URA CNRS 452, B. P. 108, 59652 Villeneuve d'Ascq Cedex, France

Received December 29, 1995; accepted April 15, 1996

The mixed-valence $PbPt_2O_4$ compound was synthesized both by solid state reaction between stoichiometric amounts of PbO and Pt heated at 650–750°C for 1 week and by chemical attack of Pb_2PtO_4. It decomposes to PbO and Pt at 750°C. The crystal structure was completely solved from direct methods and difference Fourier maps from powder X-ray diffraction data. The unit cell is triclinic (space group $P\bar{1}$, $Z = 2$) with $a = 6.1161(2)$ Å, $b = 6.6504(2)$ Å, $c = 5.5502(2)$ Å, $\alpha = 97.178(2)°$, $\beta = 108.803(2)°$, and $\gamma = 115.241(2)°$. The structural model was refined using the Rietveld profile technique and led to the reliability factors $R_{wp} = 0.118$, $R_p = 0.086$, $R_{Bragg} = 0.029$, $R_F = 0.018$, and $\chi^2 = 1.51$. The structure of $PbPt_2O_4$ appears to be a unique one involving both Pt^{4+} in octahedral coordination and Pt^{2+} or partially oxidized platinum in square-planar coordination. The $PbPt_2O_4$ structure consists of columnar-stacked PtO_4 groups extending along the c axis of the unit cell. These columnar stacks are held by other planar PtO_4 groups to constitute Pt_3O_8 sheets. These sheets are linked together by PtO_6 octahedra to form a three-dimensional framework. Lead atoms are surrounded by six oxygens forming a distorted octahedron. Metallic conductivity in $PbPt_2O_4$ is consistent with short Pt–Pt bonds in the columnar stacks of PtO_4 groups along the c axis direction ($d_{Pt-Pt} = 2.78$ Å).

INTRODUCTION

Many binary and ternary platinum oxides have already been chemically and structurally studied. Insulator, semiconductor, or metallic conductor platinum oxides have been reported. They can be classified in two groups based on the valence state and the environment of the platinum cation: the first constains divalent or partially oxidized platinum in planar coordination and the second fully oxidized tetravalent platinum in octahedral coordination (1). The first group of mixed-valence compounds includes $Na_xPt_3O_4$ (2–4) which owes its high conductivity to columnar stacks of PtO_4 groups extending along all three main crystallographic directions with short Pt–Pt distances. Other compounds, like $CaPt_2O_4$ (5), are two-dimensional columnar-stacked platinum oxides and present a metallic conductivity due to Pt–Pt interactions in two crystallographic directions. Two examples of structures with columnar stacks of PtO_4 squares in only one direction are known: the orthorhombic MPt_3O_6(M = Mg, Mn, Co, Ni, Zn, Cd) (6–8) ternary platinum oxides have a structure with Pt–Pt interaction along the c axis direction; $Bi_{2-x}Pb_xPtO_4$ ($0.33 \leq x \leq 0.52$) compounds contain PtO_4 infinite chains in the [001] direction of the tetragonal cell (9, 10). For these materials, conductivity decreases with decreasing temperature characteristic of semiconducting behavior as in other known 1D platinate conductors such as POTCP (partially oxidized tetracyano platinates) which contain stacked $Pt(CN)_4$ groups to form linear metal–atom chains with short interatomic Pt–Pt spacing (2.89 Å in KCPBr (11)). Bi_2PtO_4 cannot be synthesized; introduction of lead stabilizes the $Bi_{2-x}Pb_xPtO_4$ phase ($0.33 \leq x \leq 0.52$) whose structure is similar to that of Bi_2CuO_4 (12) and Bi_2PdO_4 (13); therefore partial oxidation of Pt^{2+} is necessary for the stability of the compound. At the other end ($x = 2$), Pb_2PtO_4 was obtained (14). The structure of Pb_2PtO_4 was solved from single-crystal X-ray diffraction data and consists of chains of edge-shared PtO_6 rutile-type octahedra extending along the c axis direction of the orthorhombic cell. Pb_2PtO_4 contains fully oxidized tetravalent platinum and, as expected, is an insulator.

Attempts to dissolve Pb_2PtO_4 in concentrated nitric acid (HNO_3 14 N), in order to determine lead and platinum contents by wet chemistry failed, but a new phase appeared which has a diffraction pattern completely different from that of Pb_2PtO_4. This new mixed platinum–lead oxide could be formulated $PbPt_2O_4$. The chemical formula indicates that platinum adopts mixed-valence states.

As no single crystals of $PbPt_2O_4$ could be obtained and structural analogies with similar compounds were not de-

[1] Present address: Laboratoire de Physicochimie des Matériaux, B.P. 1501, Oran el Menouar, Algérie.

[2] To whom correspondence should be addressed.

0022-4596/96 $18.00

tected, its crystal structure was solved from X-ray powder diffraction data.

EXPERIMENTAL

Polycrystalline $PbPt_2O_4$ was synthesized by solid state reaction of stoichiometric amounts of yellow lead monoxide (Johnson Matthey, specpure) and platinum powder (Heraeus, 99.9%) according to

$$PbO + 2\,Pt + \frac{3}{2}O_2 \xrightarrow[\text{one week}]{670^\circ C} PbPt_2O_4.$$

The mixture was well ground in an agate mortar and heated in air at 670°C for 1 week with several intermediary regrindings. The resulting dark grey powder was examined by X-ray diffraction using a Guinier–De Wolff focusing camera (Cu$K\alpha$ radiation). $PbPt_2O_4$ was also obtained from Pb_2PtO_4: about 200 mg of Pb_2PtO_4 prepared by solid state reaction between PbO and Pt at 700°C (14) was added to 20 ml of concentrated nitric acid (HNO_3 14 N). The solution became brown and after 24 h it was filtered to remove dark gray precipitated material which was identified by X-ray diffraction.

Thermogravimetric (TG) and differential thermal (DT) measurements were carried out on a 1090 DuPont Instruments thermal analyzer. Density determination was realized using an automated Micromeritics Accupyc 1330 densitometer (1 cm^3 cell). A Guinier–Lenne camera was used for high temperature X-ray investigations (HTXR). Conductivity measurements were carried out on parallelepipedic cold-pressed pellets; the four-probe method was used for the measurements which were performed between 4.2 and 300 K. Powder X-ray diffraction data used for structure determination were recorded on a Siemens D5000 $\theta/2\theta$ diffractometer, at room temperature, using Bragg–Brentano geometry, with a backmonochromatized Cu$K\alpha$ radiation. The diffraction pattern was scanned over the angle range 10°–130°(2θ) in steps of 0.03°(2θ) and a counting time of 40 s per step. Thus, the data collection required about 44 h.

As a completely random orientation of crystallites is essential in determining the true relative intensities, the sample was sifted and only particles with a size less than 40 μm were taken. Moreover, to minimize the orientation effects which occur when powdered samples are pressed, a side-loading method was used and the specimen rotated at 30 trs/mn during the measurement.

RESULTS

Thermal Stability and Formula Determination

The attack of Pb_2PtO_4 by concentrated nitric acid (HNO_3 14 N) led to a solid residue presenting a diffraction pattern completely different from that of Pb_2PtO_4. A high temperature X-ray diffraction study of this phase showed that its decomposition occurred at about 750°C giving lead monoxide and platinum metal. A TG analysis was carried out under a hydrogen stream. The reduction is achieved at 200°C and the X-ray powder diagram indicated that the reduction product was a mixture of two lead–platinum alloys, hexagonal PbPt and cubic $PbPt_{5-7}$. This result indicated that the phase contained more platinum than lead. The direct synthesis by solid state reaction between PbO and Pt was then considered. Some mixtures of different Pb/Pt ratio were realized and heated for 24 h at 670°C in air. X-ray powder diffraction patterns of the resulting products revealed that the previous phase was pure for the ratio Pb/Pt = 0.5. Thus, the new compound could be formulated $PbPt_2O_x$. DT and TG analysis realized in air on $PbPt_2O_x$ synthesized by solid state reaction, confirmed the decomposition of the phase at about 750°C. As for the HTXR study, only lead monoxide and platinum metal could be identified as decomposition products, according to the stoichiometry

$$PbPt_2O_x \rightarrow PbO + 2\,Pt + \frac{x-1}{2}O_2.$$

The weight loss measured (7.2%) corresponds to the weight increase during the formation reaction and allowed determination of the x value: $x \approx 4$. The same value is obtained from the TG analysis under hydrogen stream (weight loss 9%). A probable formula for this new phase could be written $PbPt_2O_4$. Thus the reaction of Pb_2PtO_4 into nitric acid led to a dissolution of part of the lead and a partial reduction of platinum, which seems to be more surprising. From examination of a HTXR photograph carried out in air on a sample of nominal composition PbO:2Pt, it appeared that the thermal stability domain of $PbPt_2O_4$ is weak: indeed, lead monoxide begins to react with platinum at about 650°C and decomposition occurs at about 750°C. We noticed that the domain of existence is almost the same as for Pb_2PtO_4.

Crystal Structure Determination

As the indexing of the powder pattern is a crucial stage in the powder structural analysis, a high accuracy in the determination of peaks was obtained by means of the fitting program FIT available in the PC Socabim software package DIFFRAC-AT. The first 51 lines were completely indexed by the semi-exhaustive trial-and-error powder indexing program TREOR (15). Only one probable solution in the triclinic system was proposed. The refined cell parameters using a least squares procedure are a = 6.125(2) Å, b = 6.660(2) Å, c = 5.557(2) Å, α = 97.17(2)°, β = 108.81(2)°, and γ = 115.24(2)°. The reliability of the unit

TABLE 1
X-Ray Powder Pattern of $PbPt_2O_4$ (λ_{Cu} = 1.5418 Å)

$2\theta_{obs}$	$2\theta_{calc}$	I_{obs}	h	k	l	$2\theta_{obs}$	$2\theta_{calc}$	I_{obs}	h	k	l
15.432	15.452	23	0	1	0	52.005	52.003	8	3	−3	−1
16.680	16.695	4	1	−1	0	52.166	52.167	6	0	1	−3
17.689	17.712	15	0	0	1	54.153	54.179	52	2	−2	2
19.055	19.065	6	1	0	−1	54.480	54.478	10	0	2	−3
19.646	19.640	4	0	1	−1	54.480	54.502	5	2	1	−3
26.293	26.322	33	1	−1	1	54.979	54.990	5	2	2	−2
26.678	26.693	40	1	1	−1	55.168	55.202	27	1	2	−3
26.990	26.990	40	0	1	1	55.643	55.643	50	0	2	2
27.051	27.083	31	1	−2	0	55.849	55.848	52	2	−4	0
28.816	28.841	91	1	1	0	55.739	56.720	17	2	−3	−2
29.959	29.985	84	1	0	1	57.149	57.152	6	2	1	1
30.233	30.211	41	2	−1	−1	57.525	57.511	3	2	−3	2
30.800	30.824	94	0	2	−1	57.525	57.557	3	2	−4	1
30.885	30.914	64	2	−1	0	58.896	58.873	5	3	−1	−3
31.179	31.195	78	0	2	0	58.993	59.006	17	3	1	−1
31.363	31.330	46	1	−2	1	59.599	59.578	11	3	0	−3
32.433	32.456	65	2	0	−1	59.728	59.675	10	1	3	0
32.575	32.600	16	1	0	−2	59.802	59.745	24	2	2	0
33.727	33.725	72	1	−2	−1	60.714	60.687	12	2	−2	−3
33.759	33.759	85	2	−2	0	61.601	61.594	8	0	4	−1
34.403	34.413	100	0	1	−2	62.307	62.315	21	2	0	2
35.286	35.304	59	1	1	−2	62.520	62.505	4	4	−1	−1
35.676	35.683	66	2	−2	−1	62.845	62.826	39	4	−2	−2
35.726	35.688	16	2	0	0	62.940	62.921	12	3	−2	−3
35.845	35.865	59	0	0	2	64.196	64.216	26	0	4	−2
37.195	37.202	60	1	−1	−2	64.385	64.420	13	4	−2	0
38.681	38.684	75	2	0	−2	64.555	64.589	8	1	−4	−1
39.142	39.140	28	2	−1	−2	64.778	64.787	15	3	−4	1
39.710	39.699	5	1	2	−1	64.994	65.061	5	0	4	0
39.876	39.890	14	0	2	−2	65.352	65.372	8	2	−4	2
41.240	41.311	4	2	1	−1	65.503	65.493	11	4	−3	0
41.372	41.361	4	1	−3	0	65.929	65.924	6	1	0	3
43.374	43.400	12	1	2	0	67.937	67.962	12	4	0	−2
43.714	43.679	4	1	−2	2	68.219	68.296	28	2	0	−4
45.278	45.301	16	0	3	−1	70.481	70.447	8	4	−4	−1
45.677	45.708	8	2	−2	−2	70.809	70.922	11	2	−4	−2
46.003	46.039	29	2	1	0	70.998	70.930	7	2	2	1
46.691	46.701	27	2	0	1	71.998	71.998	7	3	2	−1
46.811	46.807	7	1	0	2	72.196	72.126	4	0	1	−4
46.973	46.981	10	2	−3	1	72.305	72.272	10	1	4	−1
47.296	47.271	7	3	−2	0	72.508	72.545	18	0	2	−4
47.569	47.571	35	0	3	0	72.759	72.770	9	4	0	−3
48.146	48.198	7	1	−3	−1	73.189	73.245	4	3	−1	2
48.345	48.384	29	3	−1	0	73.877	73.912	8	4	−2	1
49.524	49.567	26	3	0	−1	74.118	74.170	11	0	4	1
50.391	50.411	11	0	3	−2	74.640	74.670	5	2	2	−4
50.632	50.642	28	1	−3	2	75.228	75.240	2	1	1	3
51.341	51.328	9	3	0	−2	75.325	75.280	8	1	−5	0
51.636	51.639	16	3	−3	0	75.538	75.581	8	4	−4	−2

cell and indexing is indicated by the conventional figures of merit $M(20) = 37$, $F_{20} = 71(0.0128,22)$ (16, 17). The indexed powder pattern is given in Table 1. No compound was found in the NIST Crystal Data with formula and cell parameters similar to those of $PbPt_2O_4$. The calculated density for $Z = 2$ is 11.94 g · cm^{-3} which is in accordance with the measured value (11.96(1) g · cm^{-3}). To extract the individual intensities from the powder pattern, a cell-constrained whole pattern fitting program was used. A characteristic of this program is that no reference to a

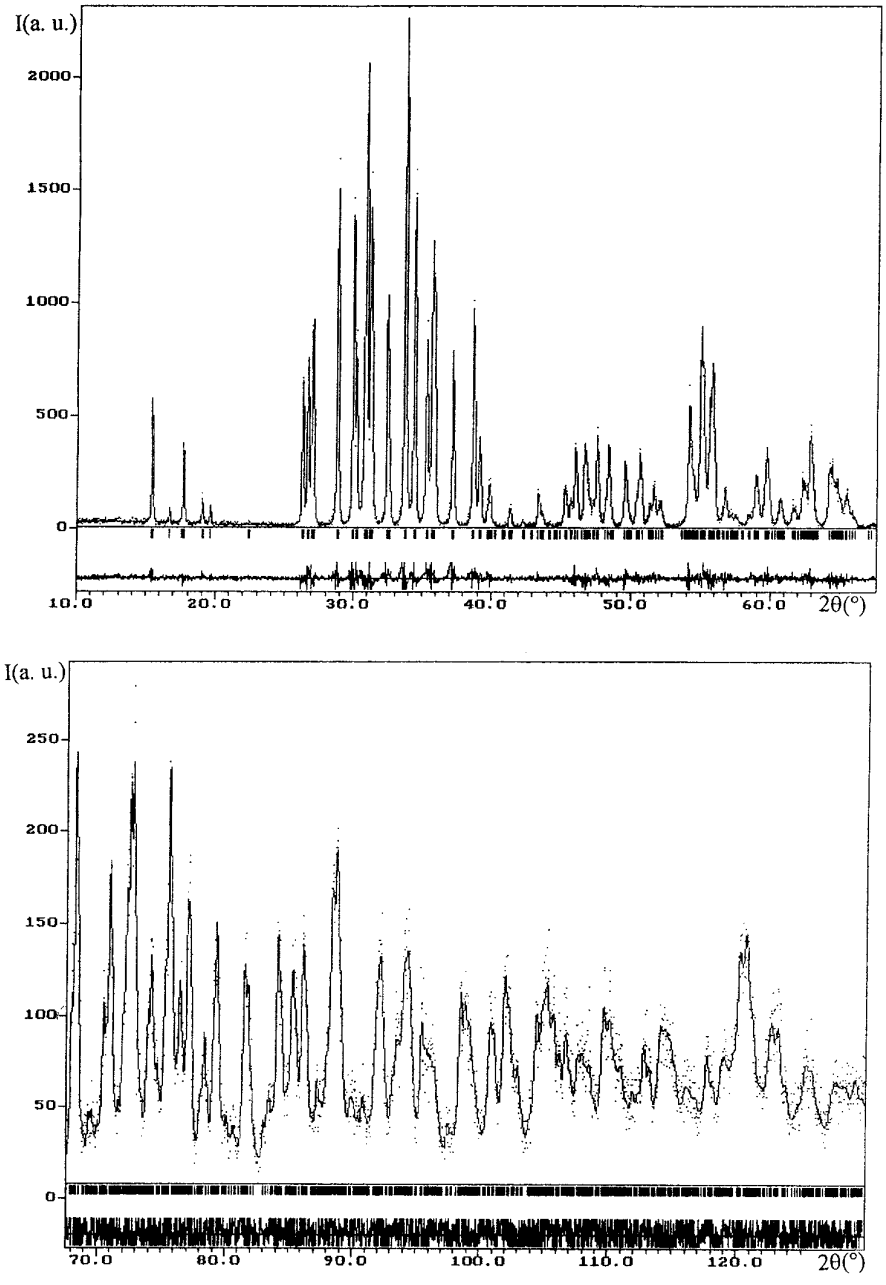

FIG. 1. Observed (points) and calculated (continuous line) X-ray diffraction patterns of $PbPt_2O_4$. The difference pattern appears in the lower part.

structural model is required, only approximate cell parameters must be provided. This method, which was first proposed by Pawley (18), allows calculation by iteration of the integrated intensities. In the present study, we used the option ''pattern matching'' included in the FULLPROF program (19). After a careful examination of the output list, 621 integrated intensities with an unambiguous indices were extracted in the range 10°–130° (2θ). Intensities were converted into structure factor amplitudes and used as input data for the SHELXS-86 program (20). Atomic scattering factors and anomalous dispersion corrections for neutral Pb, Pt, and O atoms were taken from ''International Tables for X-Ray Crystallography'' (21). Application of the automatic direct methods facilities of the SHELXS-86 program gave one general and four special positions allocated to lead and platinum atoms, respectively. This hypothesis will be further confirmed by the Pb–O and Pt–O bond length values. Successive least-squares refinements and difference Fourier maps enabled the oxygen atoms to be located. All the atom sites could

TABLE 2
Conditions of X-Ray Data Collection and Rietveld Refinement for $PbPt_2O_4$

Data Collection	
Diffractometer	Siemens D5000
Wavelengths	1.54056 and 1.54439 Å
2θ range (°)	10–130
Step scan (°2θ)	0.03
Time/step (s)	40
Results of Rietveld Refinement	
Cell parameters	a = 6.1161(2) Å; b = 6.6504(2) Å; c = 5.5502(2) Å α = 97.178(2)°; β = 108.803(2)°; γ = 115.241(2)°
Volume	V = 184.00 Å^3
Space group	$P\bar{1}$
Z	2
Number of reflections	1237
Number of refined parameters	66
Zeropoint(°2θ)	−0.0419(3)
Profile function	Pearson VII m = 1.31(7)
Halfwidth parameters	U = 0.069(6); V = 0.0145(5); W = 0.0009(9)
Asymmetry parameter	0.33(9)
$R_{wp} = [\Sigma_i w_i(y_i - y_{ci})^2/\Sigma_i w_i y_i^2]^{1/2}$	0.118
$R_P = \Sigma_i\lvert y_i - y_{ci}\rvert/\Sigma_i y_i$	0.086
$R_F = \Sigma\lVert F_{obs}\rvert - \lvert F_{calc}\rVert/\Sigma\lvert F_{obs}\rvert$	0.018
$R_{Bragg} = \Sigma\lvert I_k - I_k^{calc}\rvert/\Sigma I_k$	0.029
$\chi^2 = [R_{wp}/R_{exp}]^2$	1.51

be determined in the $P\bar{1}$ space group from the whole data set. The structure refinement was carried out with the Rietveld profile refinement technique (22, 23) by means of the program FULLPROF based on version DBW3.2S (8804) of the Rietveld code published by R. A. Young and D. B. Wiles (24). All calculations were carried out on a microVAX computer. The coordinates obtained by direct methods and difference Fourier synthesis were used as starting model in the refinement performed in the $P\bar{1}$ space group. In the present study, the peak shape was represented by a Pearson VII function with an asymmetry correction at low angles. In order to describe the angular dependence of the peak full-width at half-maximum (H), the formulation of Caglioti *et al.* (25) was used: $H^2 = U\tan^2\theta + V\tan\theta + V\tan + W$, where U, V, and W were parameters refined in the process. The background was represented by a polynomial of degree 5 in 2θ. The procedure involved the refinement of other parameters: scale factor, effective 2-theta zero of the instrument, atomic coordinates, cell parameters, individual anisotropic thermal parameters for lead and platinum atoms, and an isotropic thermal parameter constrained to the same value for all the oxygen atoms. At the end of refinement, the agreement between observed and calculated data was indicated by the reliability factors: R_{wp} = 0.118, R_p = 0.086, R_F = 0.018, and R_{Bragg} = 0.029, and by the plot of observed and calculated patterns represented in Fig. 1. The refinement converged at χ^2 = 1.51 for 1237 observations, 66 variables, and 4000 data points. The more significant factors which

TABLE 3
Atomic Coordinates and Thermal Parameters for $PbPt_2O_4$

Atom	Site	x	y	z	B_{eq} or B(Å^2)
Pb	2i	0.7500(5)	0.8609(4)	0.1430(5)	1.00[a]
Pt(1)	1g	0	1/2	1/2	0.67[a]
Pt(2)	1f	1/2	0	1/2	0.46[a]
Pt(3)	1c	0	1/2	0	0.50[a]
Pt(4)	1h	1/2	1/2	1/2	0.40[a]
O(1)	2i	0.598(6)	0.282(5)	0.350(5)	0.5(3)
O(2)	2i	0.336(6)	0.500(5)	0.120(6)	0.5(3)
O(3)	2i	0.163(6)	0.850(5)	0.176(6)	0.5(3)
O(4)	2i	0.127(6)	0.274(5)	0.481(5)	0.5(3)

[a] $B_{eq} = 4/3\,\Sigma_i\Sigma_j\beta_{ij}\,\mathbf{a}_i\cdot\mathbf{a}_j$.

TABLE 4
Anisotropic Thermal Parameters ($\beta * 10^4$) for Pb and Pt Atoms for $PbPt_2O_4$

Atom	β_{11}	β_{22}	β_{33}	β_{12}	β_{13}	β_{23}
Pb	116(13)	50(9)	78(7)	37(9)	59(11)	37(9)
Pt(1)	73(18)	39(14)	66(9)	30(13)	66(15)	45(13)
Pt(2)	44(17)	10(11)	60(9)	−1(12)	49(15)	25(13)
Pt(3)	28(19)	34(13)	53(10)	−4(13)	41(13)	30(13)
Pt(4)	22(17)	28(15)	29(9)	−2(14)	7(14)	−9(13)

TABLE 5
Selected Interatomic Distances (Å) and Angles in $PbPt_2O_4$

		Lead environment			
$Pb–O(2)^{ii}_{\bar{1}10}$	2.39(4)	O(1)–Pb–O(2)	66(1)	O(2)–Pb–O(3)	122(3)
$Pb–O(4)^{ii}_{\bar{1}11}$	2.40(3)	O(1)–Pb–O(2)	76(1)	O(2)–Pb–O(4)	70(1)
$Pb–O(3)_{\bar{1}00}$	2.51(4)	O(1)–Pb–O(3)	113(3)	O(2)–Pb–O(4)	86(2)
Pb–O(2)	2.59(4)	O(1)–Pb–O(4)	134(3)	O(2)–Pb–O(4)	139(4)
$Pb–O(1)^{ii}_{\bar{1}10}$	2.60(3)	O(1)–Pb–O(4)	142(4)	O(2)–Pb–O(4)	144(4)
$Pb–O(4)_{\bar{1}\bar{1}0}$	2.63(3)	O(2)–Pb–O(2)	67(2)	O(3)–Pb–O(4)	74(2)
		O(2)–Pb–O(3)	66(1)	O(3)–Pb–O(4)	78(2)
				O(4)–Pb–O(4)	84(1)
		Pt(1) environment			
Pt(1)–O(4) × 2	1.97(4)	O(1)–Pt(1)–O(1)	180	O(1)–Pt(1)–O(4)	101(3)
$Pt(1)–O(1)_{100}$ × 2	2.04(4)	O(1)–Pt(1)–O(4)	79(2)	O(4)–Pt(1)–O(4)	180
Pt(1)–Pt(3) × 2	2.775	Pt(3)–Pt(1)–Pt(3)	180		
		Pt(2) environment			
$Pt(2)–O(3)_{010}$ × 2	1.97(3)	O(1)–Pt(2)–O(1)	180	O(1)–Pt(2)–O(3)	96(2)
Pt(2)–O(1) × 2	2.08(3)	O(1)–Pt(2)–O(3)	84(2)	O(3)–Pt(2)–O(3)	180
		Pt(3) environment			
Pt(3)–O(2) × 2	1.95(4)	O(2)–Pt(3)–O(2)	180	O(2)–Pt(3)–O(3)	96(3)
Pt(3)–O(3) × 2	2.04(4)	O(2)–Pt(3)–O(3)	84(2)	O(3)–Pt(3)–O(3)	180
		Pt(4) environment			
Pt(4)–O(1) × 2	1.98(4)	O(1)–Pt(4)–O(1)	180	O(2)–Pt(4)–O(2)	180
Pt(4)–O(2) × 2	2.02(3)	O(1)–Pt(4)–O(2)	86(2)	O(2)–Pt(4)–O(4)	89(2)
Pt(4)–O(4) × 2	2.09(4)	O(1)–Pt(4)–O(2)	94(2)	O(2)–Pt(4)–O(4)	91(2)
		O(1)–Pt(4)–O(4)	78(2)	O(4)–Pt(4)–O(4)	180
		O(1)–Pt(4)–O(4)	102(3)		

Note. Symmetry code: (ii) $\bar{x}, \bar{y}, \bar{z}$.

represent the quality of the crystal structure model are R_F and R_{Bragg}. In this case, the results are excellent. The relatively high R_{wp} value is typically observed in Rietveld refinements from X-ray powder diffraction data. The R_{wp} factor is very sensitive to the reflection profile chosen to describe the diffraction lines (26). Moreover, the lower the relative level of the background—i.e., the greater the peak-to-noise ratio—the bigger the profile and weighted profile reliability factors (27, 28). As X-ray diffraction gives a good resolution, these factors have generally high values. We can remark that the R_p and R_{wp} factors are the conventional Rietveld ones, i.e., calculated from background-cleaned

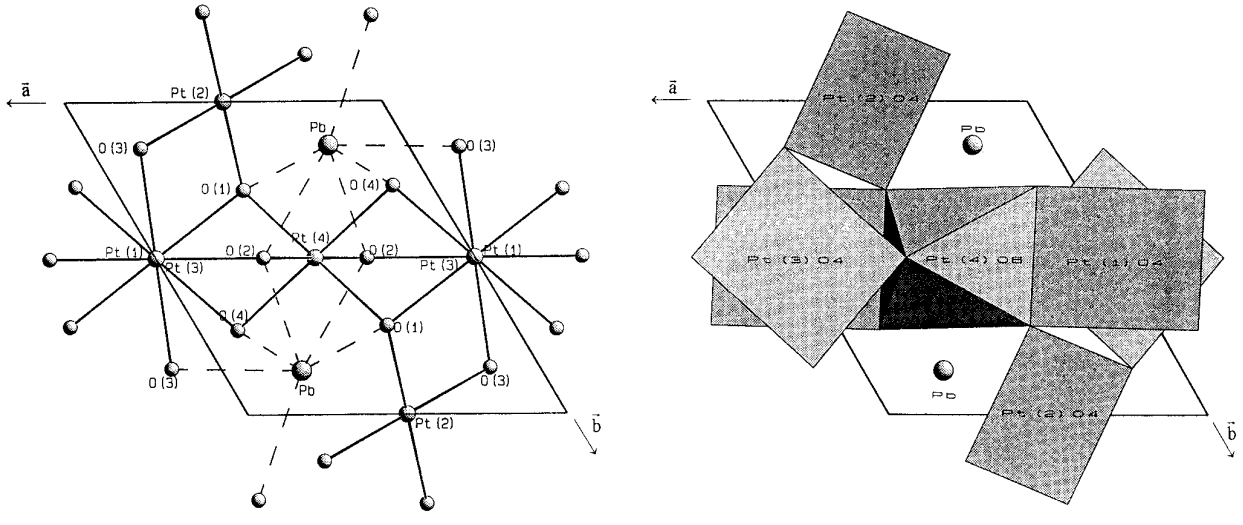

FIG. 2. Projection of the structure of $PbPt_2O_4$ along the *c* axis direction.

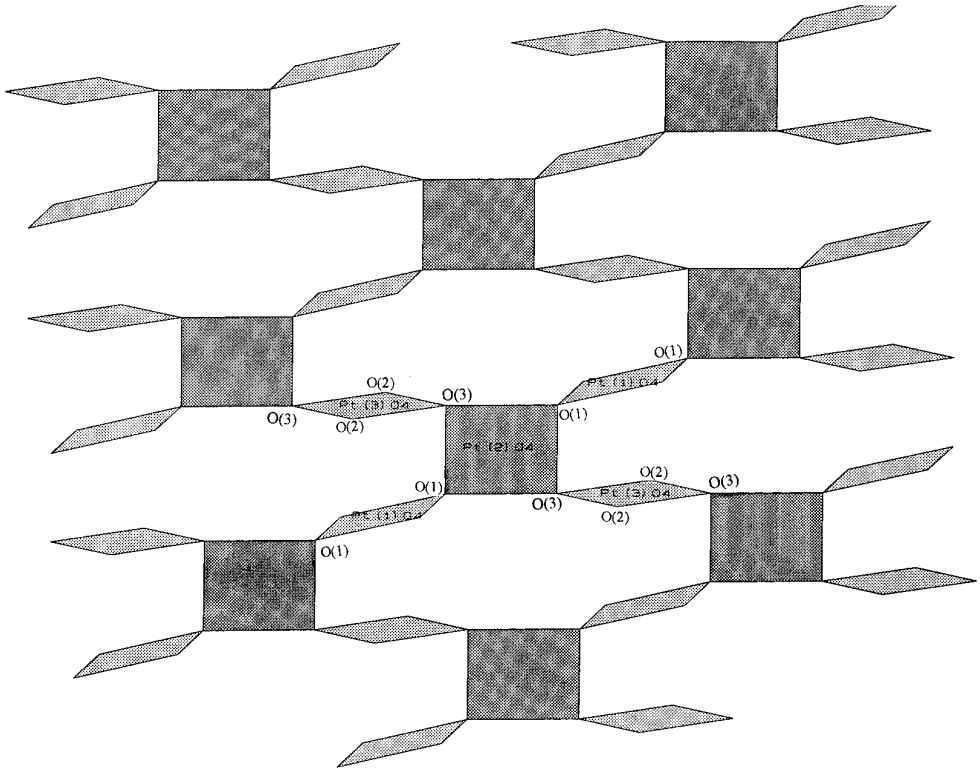

FIG. 3. $Pt(2)O_4$ polyhedron insuring intra and interchains linkage.

step intensities. Final results of the Rietveld refinement are summarized in Table 2, atomic coordinates and isotropic thermal parameters are given in Table 3, anisotropic thermal parameters are given in Table 4, and selected interatomic distances and angles are reported in Table 5.

Description of the Structure

A projection along the *c* axis direction of the structure is shown in Fig. 2. Platinum atoms present two types of environment: Pt(4) is in a regular octahedral site and Pt(1), Pt(2), and Pt(3) are in square-planar coordination. Lead atoms are in a distorted octahedral environment. $Pt(1)O_4$ and $Pt(3)O_4$ square-planes are alternatively stacked along the *c* axis direction to constitute infinite Pt–Pt chains. These square-planar groups undergo a torsion angle of about 37° around this direction to minimize anionic repulsions. The $Pt(1)O_4$ and $Pt(3)O_4$ are not parallel to each other; the angle between the perpendicular to $Pt(1)O_4$ and $Pt(3)O_4$ is 11(1)°. Square-planar $Pt(1)O_4$ and $Pt(3)O_4$ groups are linked by $Pt(2)O_4$ square planes to form infinite (Pt_3O_8) sheets parallel to the $(1\ \bar{1}\ 0)$ plane (Fig. 3). $Pt(2)O_4$ groups strengthen the intrachain cohesion and ensure the interchain cohesion; indeed, a $Pt(2)O_4$ unit shares two corners O(1) and O(3) with $Pt(1)O_4$ and $Pt(3)O_4$ units of the same columnar stack and two other corners with two groups of a parallel chain (Fig. 3). Then, these sheets are linked by $Pt(4)O_6$ octahedra to constitute a three-dimensional framework (Fig. 4). A $Pt(1)O_4$ group shares two opposite O(1)–O(4) edges with $Pt(4)O_6$ octahedra to form alternated series of octahedra and square planes along the [100] direction (Fig. 2). The $Pt(4)O_6$ octahedron exchanges its two other corners with two square-planar $Pt(3)O_4$ groups belonging to two $[PtO_4]_\infty$ chains. Thus, $Pt(4)O_6$ takes part in the Pt(1)–Pt(3) interchain cohesion. The structure of $PbPt_2O_4$ can also be described from sheets parallel to the (100) plane, formed by $Pt(1)Pt(3)O_8$ columns linked by $Pt(4)O_6$ octahedra. These sheets are then connected by means of $Pt(2)O_4$ square planes. Each lead atom is surrounded by six oxygen atoms leading to a very distorted PbO_6 octahedron, however the $6s^2$ lone pair of Pb^{2+} is not significantly stereochemically active. Two PbO_6 octahedra are linked by a O(2)–O(2) edge to form a Pb_2O_{10} group (Fig. 5). This last one ensures cohesion between the different platinum polyhedra and, in particular, links the $Pt(4)O_6$ octahedra to form chains parallel to the *c* axis. Each PbO_6 polyhedron shares one O(1)–O(2) edge with a $Pt(4)O_6$ octahedron and one O(2)–O(4) edge with another $Pt(4)O_6$ unit shifted by **c** with respect to the previous one (Fig. 5). One octahedron has one O(2)–O(3) edge in common with a $Pt(3)O_4$ unit and one corner O(4) with a $Pt(1)O_4$ belonging to the same $[PtO_4]_\infty$ chain. Another

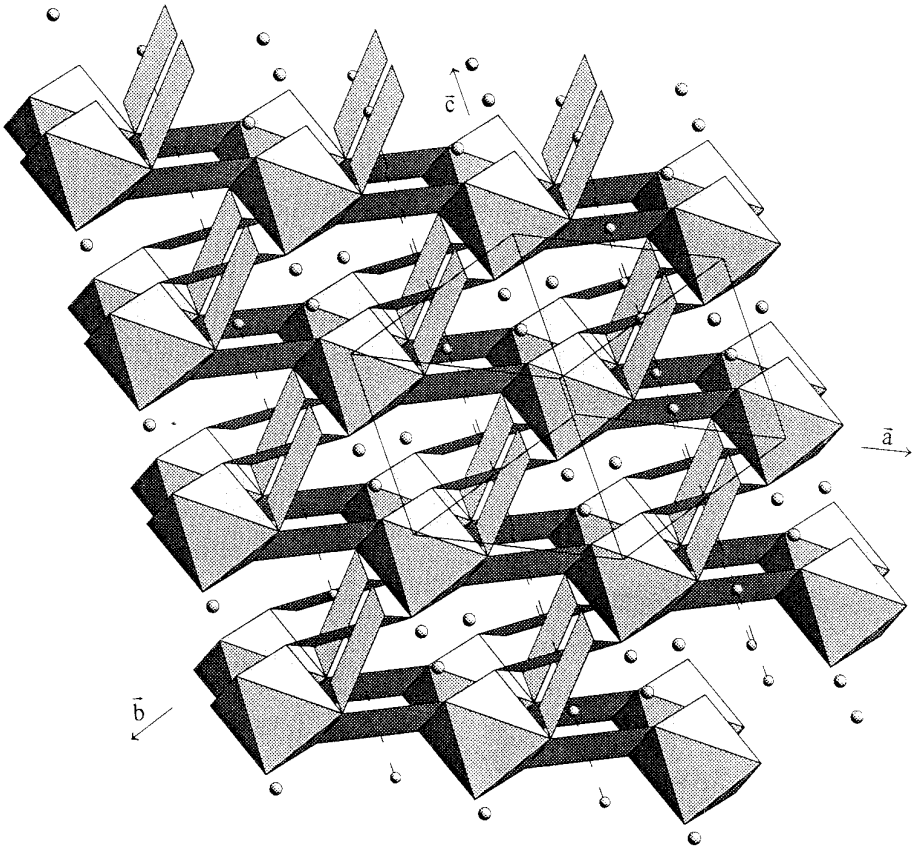

FIG. 4. View in perspective of the structure of $PbPt_2O_4$.

corner O(1) is common to a $Pt(1)O_4$ polyhedron of the $[PtO_4]_\infty$ chain shifted by **a** with respect to the previous one. PbO_6 completes cohesion within a columnar stack and between two $[PtO_4]_\infty$ neighboring chains (Fig. 2).

DISCUSSION

As usual for structures determined from X-ray powder diffraction, one cannot expect a high precision of the oxygen atom coordinates when heavy atoms are present, particularly when the heavy atoms are lead and platinum. However, the distances in Table 5 and especially the mean metal–oxygen distances are in good agreement with the values generally observed. The mean Pt–O distances for the PtO_4 groups (2.00 Å for Pt(1) and Pt(3) and 2.02 Å for Pt(2)) compare well with the sum of the Pt^{2+} in square-planar coordination and O^{2-} ionic radii (2.00 Å) (29). Similarly the mean Pt(4)–O distance (2.03 Å) is in agreement with predicted value based on an ionic radius of 0.625 Å for Pt^{4+} (VI) and confirms the oxidation state of Pt(4); the ionic radius of Pt^{2+} in six doordination is 0.80 Å. The Pb–O distance (2.52 Å) is close to $Pb^{2+}(VI) + O^{2-} = 2.59$ Å.

In the columnar stacks of Pt atoms the Pt(1)–Pt(3) distance which is half of the *c* parameter (2.78 Å) is equal to twice the metallic radius of platinum. This short Pt–Pt distance is indicative of metallic conductivity enhanced by partial oxidation of the platinum atoms. Indeed, if we assumed that Pt(4) in octahedral coordination is tetravalent and that Pt(2) in isolated square planes is divalent, the mean oxidation state of Pt(1) and Pt(3) is +3. Bond length/bond strength calculations using the method of Brown and Shannon (30) and the data of Brown and Altermatt (31) for Pt^{2+} and Pt^{4+} give a value of +4.02 for Pt(4) and +1.98 for Pt(2) (Table 6); for Pt(1) and Pt(3), the

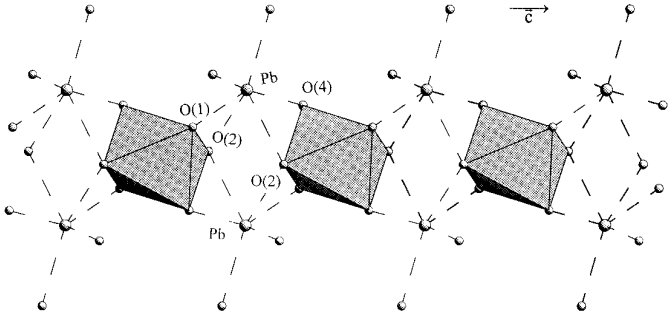

FIG. 5. Pb_2O_{10}–$Pt(4)O_6$ linkage along the (001) direction.

TABLE 6
Bond-Valence Calculation for Pt^{4+} and Pt^{2+} in $PbPt_2O_4$

Atom	Supposed bond valence	Calculated bond valence
Pt(1)	+2	+2,07
Pt(1)	+4	+2,86
Pt(3)	+2	+2,14
Pt(3)	+4	+2,94
Pt(2)	+2	+1,98
Pt(2)	+4	+2,73
Pt(4)	+2	+2,84
Pt(4)	+4	+4,02

results are less significant, however they seem to indicate a partial oxidation of Pt^{2+}. The sum of the electrostatic valence for the lead atom is calculated to be +2.06.

As expected, the electrical conductivity of $PbPt_2O_4$ measured on sintered powder decreases with increasing temperature, characteristic of metallic behavior (Fig. 6).

Similar strong Pt–Pt interaction exists in columnar stacks of PtO_4 groups found in several other compounds. For example, in the $Bi_{2-x}Pb_xPtO_4$ phase ($0.33 \leq x \leq 0.52$), the Pt–Pt distance decreases from 2.834 to 2.816 Å with increasing x (10); the conductivity of these compounds decreases with decreasing temperature characteristic of semiconductivity behavior although metallic conductivity would be expected due to strong interaction and mixed-valence of platinum. Other examples are provided by the one-dimensional cyano or oxalato platinum complexes. Thus $K_2[Pt(CN)_4] \cdot 3H_2O$ is a colorless solid, but by appropriate partial oxidation it is possible to obtain cation deficient [i.e., $K_{1.75}[Pt(CN)_4] \cdot 1.5H_2O$] and other partially oxidized compounds such as KCP(Br) ($K_2Pt(CN)_4Br_{0.3} \cdot 3H_2O$) (11). In these compounds, square-planar $[Pt(CN)_4]$ ions are stacked to give a linear chain of Pt atoms in which the Pt–Pt distances of 2.80–3.00 Å allow strong overlap of the dz^2 orbitals. This accounts for high conductance along the crystal axis. In MPt_3O_6 compounds (M = Mg, Ca, Mn, Fe, Co, Ni, Cu, Zn, Cd, Hg) (6) the columnar stacks of PtO_4 groups extending along the c axis of the orthorhombic cell are held together by edge-shared PtO_6 octahedra. The Pt–Pt distances along c are between 3.10 and 3.16 Å. Nonstoichiometry leads to partial oxidation of the columnar stacks and enhances conductivity. For all these compounds the conductivity decreases with decreasing temperature; however σ is high with low activation energy, yielding evidence on the inherent instability of 1D electrical conduction and the distortion of the system which result in lower symmetry and a splitting of the partially filled band (Peierls distortion). In the series of metallic platinum oxides with $Na_xPt_3O_4$ structure (platinum bronze structure) strong Pt–Pt interactions occur in columnar-stacked PtO_4 groups extending along the three cubic axes; the Pt–Pt distances are 2.80 Å in $Na_{0.25}Pt_3O_4$ and 2.84 Å in $Na_{1.0}Pt_3O_4$. In the $CaPt_2O_4$ compound, one Pt–Pt chain is missing, the unit cell becomes tetragonal, and the crystal structure involves nonintersecting Pt chains in the a and b directions with Pt atoms slightly paired with Pt–Pt alternate distances of 2.79 and 2.99 Å; the mean oxidation state of the platinum atom is +3, like Pt(1) and Pt(3) in $PbPt_2O_4$.

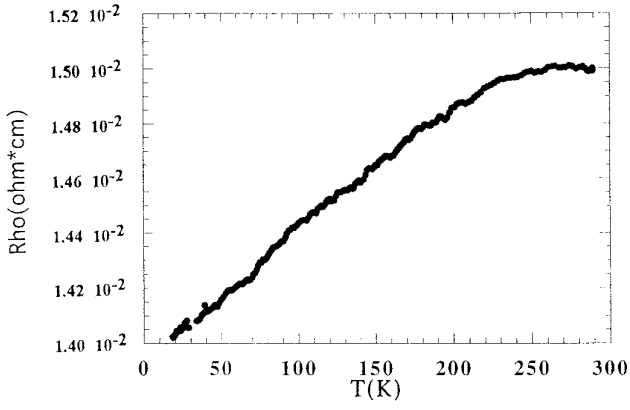

FIG. 6. Variation of resistivity versus temperature in $PbPt_2O_4$.

$PbPt_2O_4$ is the third compound isolated in the Pb–Pt–O ternary system with Pb_2PtO_4 (14) and the platinate pyrochlores $Pb_2Pt_2O_{7-x}$ (32, 33). These previously reported lead–platinum oxides contain only octahedrally coordinated Pt^{4+} and are insulators or semiconductors. In Pb_2PtO_4, chains of edge-shared $Pt^{4+}O_6$ octahedra extending along the c direction of the orthorhombic cell are bridged by Pb^{2+} ions; the Pt–Pt distance along the chain is 3.14 Å, but coordination and valence state of platinum preclude metallic conductivity. In the pyrochlores, the Pt–Pt distance between corner-shared PtO_6 octahedra is about 3.6 Å; the presence of Pt^{4+}, once again, inhibits metallic behavior.

Substitution of other M^{4+} ions for Pt(4) and Cu^{2+} for Pt(2) and/or Pt(1), Pt(3) are planned. Moreover, in the $Bi_{2-x}Pb_xPtO_4$ series, the mean oxidation degree of platinum is controlled by x, so the substitution of Bi^{3+} for Pb^{2+} in $PbPt_2O_4$ could lead to partial reduction of Pt(1) and Pt(3). The effects of these substitutions on conductivity properties will be investigated.

REFERENCES

1. K. B. Schwartz and C. T. Prewitt, *J. Phys. Chem. Solids* **45,** 1 (1984).
2. J. Waser and E. D. McClanahan, *J. Chem. Phys.* **19,** 413 (1951).
3. J. Waser and E. D. McClanahan, *J. Chem. Phys.* **20,** 199 (1952).
4. K. B. Schwartz, C. T. Prewitt, R. D. Shannon, L. M. Corliss, J. M. Hastings, and B. L. Chamberland, *Acta Crystallogr. B* **38,** 363 (1982).
5. D. Cahen, J. A. Ibers, and M. H. Mueller, *Inorg. Chem.* **13,** 110 (1974).
6. R. D. Shannon, *U.S. Patent* 3663181 (1972).

7. C. T. Prewitt, K. B. Schwartz, and R. D. Shannon, *Acta Crystallogr. C* **39,** 519 (1983).
8. K. B. Schwartz, J. B. Parise, C. T. Prewitt, and R. D. Shannon, *Acta Crystallogr. B* **39,** 217 (1983).
9. J. C. Boivin, P. Conflant, and D. Thomas, *Mater. Res. Bull.* **11,** 1503 (1976).
10. N. Bettahar, P. Conflant, J. C. Boivin, F. Abraham, and D. Thomas, *J. Phys. Chem. Solids* **46(3),** 297 (1985).
11. K. Krogmann and H. D. Hausen, *Z. Anorg. Allg. Chem.* **358,** 67 (1968).
12. J. C. Boivin, J. Trehoux, and D. Thomas, *Bull. Soc. Fr. Miner. Cristallogr.* **99,** 193 (1976).
13. P. Conflant, J. C. Boivin, and D. Thomas, *Rev. Chim. Min.* **14,** 249 (1977).
14. N. Bettahar, P. Conflant, F. Abraham, and D. Thomas, *J. Solid State Chem.* **67,** 85 (1987).
15. P. E. Werner, L. Erikson, and M. Westdhal, *J. Appl. Crystallogr.* **18,** 367 (1985).
16. P. M. De Wolff, *J. Appl. Crystallogr.* **1,** 108 (1968).
17. G. S. Smith and R. L. Snyder, *J. Appl. Crystallogr.* **12,** 60 (1979).
18. G. S. Pawley, *J. Appl. Crystallogr.* **14,** 357 (1981).
19. J. Rodriguez Carvajal, M. T. Fernandez Diaz, and J. L. Martinez, *J. Phys. Cond. Matter.* **3,** 3215 (1991).
20. G. M. Sheldrick, *in* "Crystallographic Computing 3" (G. M. Sheldrick, C. Krüger, and R. Goddard, Eds.), p. 175. Oxford Univ. Press, London, 1985.
21. "International Tables for X-ray Crystallography," Vol. IV. Knock Press, Birmingham, 1974.
22. H. M. Rietveld, *Acta Crystallogr.* **22,** 151 (1967).
23. H. M. Rietveld, *J. Appl. Crystallogr.* **2,** 65 (1969).
24. D. B. Wiles and R. A. Young, *J. Appl. Crystallogr.* **14,** 149 (1981); *J. Appl. Crystallogr.* **15,** 430 (1982).
25. C. Caglioti, A. Paoletti, and E. P. Ricci, *Nucl. Instrum. Meth.* **3,** 223 (1958).
26. R. A. Young and D. B. Wiles, *J. Appl. Crystallogr.* **15,** 430 (1982).
27. R. J. Hill, *J. Appl. Crystallogr.* **25,** 589 (1992).
28. E. Jansen, W. Schäfer, and G. Will, *J. Appl. Crystallogr.* **27,** 492 (1994).
29. R. D. Shannon, *Acta Crystallogr. A* **32,** 751 (1976).
30. I. D. Brown and R. D. Shannon, *Acta Crystallogr. A* **29,** 266 (1973).
31. I. D. Brown and D. Altermatt, *Acta Crystallogr. B* **41,** 244 (1985).
32. V. B. Lazarev and I. S. Shaplygin, *Russ. J. Inorg. Chem.* **23,** 163 (1978).
33. A. W. Sleight, *Mater. Res. Bull.* **6,** 775 (1971).